**Atmospheric
Chemistry
and Physics
Discussions**

Aerosol radiative
forcing over land
from meteosat-7

T. Elias and J.-L. Roujean

Title Page	
Abstract	Introduction
Conclusions	References
Tables	Figures

◄◄	►►
◄	►
Back	Close

Full Screen / Esc

Printer-friendly Version

Interactive Discussion

EGU

Estimation of the aerosol radiative forcing at ground level, over land, and in cloudless atmosphere, from METEOSAT-7 observation: method and first results

T. Elias[1] and J.-L. Roujean[2]

[1]LMD, Ecole Polytechnique, 91128 Palaiseau cedex, France
[2]CNRM/GMME/MATIS, Meteo-France, 42, avenue G. Coriolis, 31057 Toulouse cedex, France

Correspondence to: T. Elias (thierry.elias@lmd.polytechnique.fr)

Aerosol radiative forcing over land from meteosat-7

T. Elias and J.-L. Roujean

Printer-friendly Version

Interactive Discussion

EGU

Abstract

A new method is proposed to estimate the spatial and temporal variability of the solar radiative flux reaching the surface (DSSF) over land, as well as the Aerosol Radiative Forcing (ARF), in cloud-free atmosphere. The objective of global applications of the method is fulfilled by using the visible broadband of METEOSAT-7 satellite which scans Europe and Africa on a half-hourly basis. The method relies on a selection of best correspondence between METEOSAT-7 radiance and DSSF computed with a radiative transfer code.

The validation of DSSF is performed comparing retrievals with ground-based measurements acquired in two contrasted environments, i.e. an urban site near Paris and a continental background site in South East of France. The study is concentrated on aerosol episodes occurring around the 2003 summer heat wave, providing 42 cases of comparison for variable solar zenith angle (from 59° to 69°), variable aerosol type (biomass burning emissions and urban pollution), and variable aerosol optical thickness (a factor 6). The method reproduces measurements of DSSF within an accuracy assessment of 20 Wm^{-2} (5% in relative) in 70% of the cases, and within 40 Wm^{-2} in 90% of the cases.

Considering aerosol is the main contributor in changing the measured radiance at the top of the atmosphere, DSSF temporal variability is assumed to be caused only by aerosols, and consequently the ARF at ground level and over land is also retrieved: ARF is computed as the difference between DSSF and a parameterised aerosol-free reference level. Retrievals are linearly correlated with the ground-based measurements of the aerosol optical thickness (AOT): sensitivity is included between 120 and 160 Wm^{-2} per unity of AOT at 440 nm. AOT being an instantaneous measure indicative of the aerosol columnar amount, we therefore prove the feasibility to infer instantaneous aerosol radiative impact at the ground level over land with METEOSAT-7 visible channel.

EGU

1 Introduction

Incoming solar radiation at the bottom of the atmosphere (called DSSF for Downwelling Surface Solar radiative Flux) is steering major processes of the surface-atmosphere interface such as surface heating, evaporation rate, and plant growth. DSSF is strongly dependent on the composition of the atmosphere since its elements enact absorption and scattering back to space of part of the solar radiation. Molecules scatter radiation according to the Rayleigh theory, and some molecules such as water vapour absorb radiation. Scattering and absorbing properties of suspended particles, which are aerosols and cloud droplets, depend on their number, size, chemical composition, and shape. Spatial and temporal heterogeneity of cloud, aerosol and water vapour fields induce the high variability of DSSF. The survey of DSSF variability was early recognised as an essential duty in meteorology and networks of ground-based pyranometer instruments were deployed to quantify the available solar energy at the ground level. However a large number of geographic areas remained poorly sampled. Spatial technology developed which promised a global consistent geographic coverage from spatial remote sensing. An overview of the methods of satellite-based estimations of DSSF is given by Schmetz (1989).

A clear understanding of the causes of the current climate change is jeopardized by the prevalent uncertainty on the role of aerosols on DSSF and on the Earth's albedo. This is due to the difficulty in simulating aerosol flux emission and deposition, as well as their transformation in the atmosphere. Resolving this issue requires to link observations of changes in the atmosphere composition to observations of change in the radiative budget. In this context, remote sensing from satellite platforms is the only way to survey the high spatial heterogeneity of aerosol properties. However it is difficult to discriminate, in the ascending signal, between the competitive contributions of 1) the radiation back-scattering by aerosols and 2) the surface reflection. Several methods have been proposed to improve the precision on the Aerosol Radiative Forcing (ARF) estimated at ground level and at the Top Of the Atmosphere (TOA).

The only approach referred by IPCC in 2001 for providing global estimates of ARF at TOA lies on the Global Circulation Modelling. Later, Yu et al. (2006) offer a review of most recent studies, on the behalf that "it is now feasible to shift the estimates of aerosol forcing from largely model-based to increasingly measurement-based". For example Zhou et al. (2005) derive ARF at both TOA and ground levels for main world-wide aerosol types using AERONET retrieved aerosol models. Even if some aspects of the aerosol parameters as the aerosol vertical profile have to be assumed, this is the most precise method to evaluate the aerosol radiative effect at ground level. However AERONET can not ensure a global coverage. Chung et al. (2005) combine three data sets to estimate ARF at surface and at TOA: i) AERONET network measurements; ii) MODIS satellite observation; iii) the GOCART chemistry-transport model. The draw-back of such approach is the difficulty in guaranteeing the compatibility of the three sets of hypotheses.

Yu et al. (2006) advocate exhaustive sampling of the angular, spectral and polarising properties of upwelling radiation for increasing the precision of ARF over land. How-ever such data set is acquired only once a day and diurnal variations of both the aerosol loads and the cloud cover stay unknown. The high frequency of the observations from the meteorological geostationary platforms avoids making hypothesis on the diurnal cycle of aerosols and clouds. Several studies prove the feasibility to provide global estimate of ARF based on the wealth of data provided by the METEOSAT instrument series. For example, Costa and Silva (2005) provide aerosol optical thickness and aerosol radiative forcing at TOA, processing the data set acquired over land from the METEOSAT Second Generation instruments, exploiting the enhanced spectral capa-bilities. Their method can not be reported on the archive database acquired during the end of the 20th century by the first generation instruments. Thieuleux et al. (2005) also process data sets from the new generation instruments to derive an aerosol product, but for ocean pixels.

This paper proposes a method to provide an estimate of DSSF in cloud-free sky and over land, by using the unique data set acquired in the solar spectrum broadband

EGU

channel by the instrument onboard the METEOSAT-7 satellite, belonging to the first instrument generation mounted on meteorological geostationary spatial platforms. The high frequency of METEOSAT-7 observation allows estimating the temporal variability of DSSF and in particular the contribution of aerosols in this variability: the difference
5 between DSSF result and a computed aerosol-free reference provides ARF. The principle of the method lies on the energy conversion of measured TOA reflectance into surface radiative flux, through a Look Up Table generated with the 6S radiative transfer code (Vermote et al., 1997), and following a sequential procedure to discern aerosol from surface signatures, based on analysis of the angular dependence of the TOA sig-
10 nal. The method has been developed in the context of the operational FP6/**geoland** project which aims the global retrieval of DSSF. Technical description is given by Elias and Roujean (2006). This paper shows results of DSSF and ARF over two predetermined sites for validation purposes of the algorithm. Section 2 presents a sensitivity study of DSSF, computed with a radiative transfer code. Section 3 presents the method
15 and first results are compared to ground-based measurements in Sect. 4, for validation purposes of satellite-based estimates of DSSF and ARF.

2 Downwelling Surface Solar radiative Flux

The Downwelling Surface Solar radiative Flux (DSSF) is the component of the solar radiation reaching the Earth's surface. DSSF is composed of: i) the transmitted solar
20 radiation; ii) the radiation scattered by the atmosphere; and iii) the radiation reflected by the surface and back-scattered downwards by the atmosphere. DSSF is the spectral integration of the downwelling flux over the solar spectral interval [$0.3\,\mu$m; $4\,\mu$m] and is counted in units of Wm^{-2}.

The main factors affecting DSSF were early clearly identified: e.g. Schmetz (1989)
25 notes that "clouds are the strongest modulators of the shortwave radiation fields", together with the sensitivity to the solar zenith angle (SZA). From this statement, operational methods focussed on cloud radiative effects with the objective to infer continuous

fields of DSSF from geostationary satellite measurements, neglecting aerosol impacts. In cloud-free sky conditions, DSSF is most sensitive to the aerosols as it is showed by computations with the 6S radiative transfer code (Vermote et al., 1997), by varying the aerosol optical properties which are: the optical thickness (AOT), that is proportional to

5   the aerosol column concentration; the single scattering albedo (ASSA) which describes the radiation absorbing property; and the Ångström exponent (AE), which depends on the size distribution respecting the Junge law. Figure 1 shows the sensitivity of DSSF to AOT at 550 nm (AOT550) for two values of ASSA, two values of AE, and for SZA=30° (Fig. 1a) and for SZA=60° (Fig. 1b). Figure 1 outlines the decrease of DSSF when

10 AOT550 increases. The decrease is modulated by both values of ASSA and AE. For SZA=60°, according to ASSA and AE, DSSF is reduced by 100 to 230 Wm^{-2} per unity of AOT550, which represents between 20% and 45% of the signal. The decrease can be larger for SZA=30°, reaching 300 Wm^{-2}, which is 30% of the aerosol-free level. Surface albedo (SAL) shows little influence on DSSF as its contribution necessitates

15 multiple scattering. Other computations are made varying successively water vapour and ozone concentrations, keeping constant other parameters, and for an aerosol-free atmosphere (not shown): the DSSF sensitivity is smaller than 1% per 100 Dobson Units (DU) of ozone and is around 2% per gcm^{-2} of water vapour.

An aerosol-free reference can be estimated by taking up the parameterisation ap-
20 proach. For example, the clear-sky algorithm in the Ocean & Sea Ice SAF project, implemented by Gautier et al. (1980) according to the method of Lacis and Hansen (1974), is formulated as follows:

$$DSSF_{par} = K_{esd}E_{Sun}\mu_S T \tag{1}$$

E_{Sun} is the extra terrestrial solar irradiance over the wavelength range [0.3 μm, 4 μm],
25 K_{esd} is the correction factor for the varying distance between Earth and sun, and μ_S is the cosine of the solar zenith angle. Aerosols, water vapour and ozone are taken into account for calculating the downwelling atmospheric transmittance T (Appendix A) $DSSF_{par}$ is calculated for an aerosol-free atmosphere (δ=0) where gaseous absorption is defined by ozone concentration of 300 DU and water vapour concentration of

2 gcm^{-2}, and is plotted in function of SZA in Fig. 2. Difference between the 6S radiative transfer code and the parameterization is negligible for pure Rayleigh atmosphere.

ARF for SZA=60° is calculated by subtracting 6S-computed DSSF to the parameterised aerosol-free reference level and is plotted in Fig. 3 in function of AOT440.
ARF is highly dependent on the aerosol optical properties. The dependence to AOT is closely linear, with a slope varying between 80 Wm^{-2} for an accumulation-mode dominated and non-absorbent aerosol population, to 140 Wm^{-2} for an accumulation-mode dominated and absorbent aerosol population and to 200 Wm^{-2} for a coarse-mode dominated and absorbent aerosol population.

3   The method

3.1   Principle

Radiative processes inside the Surface-Atmosphere System (SAS) can not be resolved from a single measurement: realistic radiative transfer computation of DSSF can not be made considering METEOSAT-7 as unique source of information. Consequently the principle of our method lies on an energetical conversion from the METEOSAT-7 measurement (written UTVR$_{meas}$ for measured Upwelling TOA Visible Radiance) to the DSSF result (written as DSSF$_{res}$), ignoring the exact description of the SAS generating both values of METEOSAT-7 measurement and DSSF$_{res}$.

The core of the problem consists in establishing a universal relationship between UTVR$_{meas}$ and DSSF$_{res}$. Empirical methods were early proposed (Schmetz, 1989), however the spatial scale of applicability is limited as the training data set can not represent the wide number of contrasted situations occurring worldwide. The alternative method which is chosen in this study is to generate Look Up Table (LUT) of DSSF and UTVR values, spanning numerous realistic SAS models as input of a numerical radiative transfer code. The definition of DSSF$_{res}$ from the LUT is not trivial as several SAS models are candidate to reproduce the unique value of UTVR$_{meas}$, which generate dif-

ferent values of DSSF. Constrains are necessary to reduce the number of candidate SAS models and consequently to reduce the range of values of candidate DSSF.

It is noticed that dependence of UTVR on SAL increases with decreasing SZA and oppositely dependence of UTVR on AOT increases with increasing SZA. Then, the high frequency of the METEOSAT-7 measurements is exploited to discriminate between the aerosol and surface contributions to $UTVR_{meas}$: measurements made at minimum value of SZA (local noon) are devoted to operate a restitution of SAL; in counterpart, off-nadir measurements are intended to document AOT. The treatment process is then sequenced: step 1) noon measurements provide indication on the surface optical properties (SAL), which is, step 2), reported on all measurements to get information on AOT; step 3) AOT and $UTVR_{meas}$ are two constraints for selecting the candidate SAS models; 4) DSSF is calculated for the candidate SAS models; 5) candidate DSSF values are averaged to give $DSSF_{res}$ (steps summarised in Table 2). Assuming the surface properties are stationary on a monthly basis, all measurements made at noon during the month are first analysed to derive a monthly value of SAL, which is then reported to analyse all other measurements to infer instantaneous $DSSF_{res}$. The description of the algorithm is shared out between Sect. 3.2, for the LUT generation, and Sect. 3.3, for looking for the best correspondence between $UTVR_{meas}$ and $DSSF_{res}$.

3.2 Generation of the LUT

LUT of both values of $DSSF_{LUT}$ and $UTVR_{LUT}$ is generated with the 6S radiative transfer code by varying input parameters which describe the SAS models and the geometry.

3.2.1 The Surface Atmosphere Systems models

The SAS models are defined by varying 4 parameters (Table 1). Surface reflection is represented by its albedo SAL. The aerosol is represented by three parameters describing extinction (AOT), absorption (ASSA or the Imaginary Refractive Index IRI) and the averaged particle size (AE or the Aerosol Size Distribution slope ASD). ASD is the

EGU

slope of the size distribution respecting the Junge law, proportional to the Ångström exponent AE. 6S radiative transfer computations are made for each SAS model, each delivering one value of $DSSF_{LUT}$ and one value of $UTVR_{LUT}$ for one observation geometry.

5   As is summarised in Table 1, SAL varies between 0.05 and 0.40 with an increment of 0.05. SAL is spectrally defined over the METEOSAT-7 visible channel. AOT is defined at 550 nm, it varies between 0.05 and 1.50 with an increment of 0.10 from 0.10 to 1.50 and a first increment of 0.05. This AOT interval includes most conditions observed worldwide (Holben et al., 2001). ASD takes both values of 3.50 and 4.75, and IRI

10   the three values of 0.001, 0.015 and 0.030. All combinations of the geophysical input parameters deliver 768 SAS models (8×16×2×3). However some combinations are not realistic. Coarse-mode dominant particles are not absorbent when they are few, because they represent maritime particles. Coarse-mode dominant particles are always absorbent when they are many since they represent desert dust particles. These

15   characteristics are translated by these 2 conditions, respectively: 1) IRI=0.001 when ASD=3.50 and AOT≤0.20; 2) IRI≥0.015 when ASD=4.75 and AOT≥0.20. No conditions are imposed when ASD=4.75. Water vapour and ozone concentrations are kept constant. The final number of SAS models is 632.

3.2.2 The geometry

20   The FP6/**geoland** LUT considers all possible observation geometries, given a spatial geostationary platform: all pixels over the METEOSAT-7 disk, and all time of the day during a full year. The observation geometry consists in the combination of viewing and solar angles. A 1°-resolution in viewing and solar angles is required. The 6S code is run to provide a 10°-resolution and polynomial interpolation of $DSSF_{LUT}$ and $UTVR_{LUT}$

25   provides the 1°-resolution (Elias and Roujean, 2006). The complete LUT is not necessary for the present study, and 6S computations are operated for the exact geometrical configuration corresponding to the two pixels covering the Baseline Surface Radiation Network (BSRN) stations of Carpentras (44°03′N, 05°02′E, 100 m a.s.l.) and Palaiseau

Aerosol radiative forcing over land from meteosat-7

T. Elias and J.-L. Roujean

Title Page

Abstract   Introduction

Conclusions   References

Tables   Figures

◄   ►

◄   ►

Back   Close

Full Screen / Esc

Printer-friendly Version

Interactive Discussion

EGU

(48° 42′N, 02°12′E, 156 m a.s.l.), once per day during more than a month.

3.2.3 The altitude and the spectral domain

The surface elevation affects $DSSF_{LUT}$ and $UTVR_{LUT}$ mainly by changing the Rayleigh scattering. All operations previously described are repeated, in the FP6/**geoland** algo-
5 rithm, at several altitude levels, which are chosen after a statistical study of the surface altitude over continents and a sensitivity study of $DSSF_{res}$ (Elias and Roujean, 2006). For the paper, computations are made at the unique altitude of 300 m above sea level (a.s.l), which corresponds to the lowest surface elevation range of the FP6/**geoland** algorithm, and which is close to the altitudes of both Carpentras and Palaiseau stations.
10 $DSSF_{LUT}$ and $UTVR_{LUT}$ also depend on the spectral domain of computation. The spectral function for the computation of $DSSF_{LUT}$ is defined constant all over the globe according to the FP6/**geoland** specifications, while it varies according to the spatial instrument for $UTVR_{LUT}$. For the paper, computations of $UTVR_{LUT}$ are made for the METEOSAT-7 spectral channel.

15 ## 3.3 Selecting $DSSF_{res}$ from the LUT

The following step of the method consists in deriving $DSSF_{res}$ using the LUT and $UTVR_{meas}$. $UTVR_{meas}$ is used to select the candidate SAS models which then provide an interval of $DSSF_{LUT}$ values from which $DSSF_{res}$ must be defined. The systematic criterion of selection is called $UTVR_{meas}$ cond: $|UTVR_{LUT}-UTVR_{meas}| < 10\%$ (Table 2).
20 More criteria are applied to determine $DSSF_{res}$, according to the time of acquisition of $UTVR_{meas}$ (Table 2).
First, information on the surface reflection properties is attained by analysing the candidate SAS models corresponding to the noon measurement. The most frequent value among the candidate SAL_{LUT} values is kept as SAL_{mo} (for "maximum occurrence" of
25 SAL_{LUT} values), an internal parameter considered representative of the surface properties of the pixel. This operation is repeated for all cloud-free pixels acquired at noon

Title Page

Abstract | Introduction

Conclusions | References

Tables | Figures

◄◄ | ►►

◄ | ►

Back | Close

Full Screen / Esc

Printer-friendly Version

Interactive Discussion

EGU

T. Elias and J.-L. Roujean

during the whole month in order to provide the monthly value of SAL_{mo}. This operation also provides instantaneous value of $DSSF_{res}$ which is the average of the candidate $DSSF_{LUT}$ values (Table 2).

Second, measurements made off-nadir are processed. Simulations show that a given value of UTVR can be reproduced for several values of SAL, as long as AOT is also varied. Increasing SAL and decreasing AOT allows maintaining a constant value of UTVR. Therefore by restricting SAL_{LUT}, AOT_{LUT} is also restricted. In particular the upper limit SAL_{max} matches with the lower limit AOT_{min}. Instantaneous estimate of AOT_{min} is provided by restricting SAS candidate models by the criterion: $SAL_{LUT} < SAL_{max}$ (Table 2). SAL_{max} is determined from SAL_{mo}. Because of the high anisotropy of the surface reflection, SAL_{max} is made variable from morning to afternoon: $SAL_{max} = SAL_{mo} - 0.10$ the morning, $SAL_{max} = SAL_{mo} - 0.05$ the afternoon.

Third, $DSSF_{res}$ is retrieved respecting the condition $AOT_{min} - 0.1 < AOT_{LUT} < AOT_{min} + 0.2$ (Table 2). All SAS models satisfying this further condition provide values of $DSSF_{LUT}$ which are averaged to give $DSSF_{res}$. Noon measurements are not processed in this paper, and SAL_{max} value is taken from Elias and Roujean (2006).

3.4 The cloud screening

The Institute of Climate and Meteorological Research of Karlsruhe, Germany, has developed an algorithm of cloud detection to be applied on METEOSAT-7 data, in the framework of the FP6/**geoland** objective to infer 10-days composite of $^1/_2$-hourly surface temperature, at a spatial resolution of 10 km, over Europe and Africa (FP6/**geoland** WP8316). Only clear-sky pixels are processed to deliver surface temperature, consequently the cloud mask is very strict in order to reject any pixel contaminated by cloud scattering. The cloud mask index has been validated against ground-based data sets acquired in Carpentras during the 2000 summer (Elias and Roujean, 2006). For the paper the cloud screening is based on a threshold on the temporal variability of ground-based measurements of DSSF (Sect. 4).

4 Validation of the method

METEOSAT-7 data are analysed with the algorithm to get $DSSF_{res}$ for variable atmospheric situations. The validation consists in comparing retrievals to ground-based measurements by pyranometers of both BSRN stations of Carpentras (44°03′N, 05° 02′E, 100 m a.s.l.) and Palaiseau (48°42′ N, 02°12′ E, 156 m a.s.l.). Validation of AOT_{min} is not attempted because they are dedicated to be used only as internal parameters of the algorithm. SAL_{max} is estimated at 0.15 by Elias and Roujean (2006) for both locations.

The two pixels corresponding to the two stations are selected in the METEOSAT-7 images. Temporal series of $DSSF_{res}$ is generated by considering the METEOSAT-7 slot number 14 every day during more than a month in the 2003 summer. Measurement in the slot 14 is made at 07:20 UT above France. METEOSAT-7 data are analysed when no clouds are detected by the pyranometer: Flux measured in the solar spectrum channel with the CMP11 Kipp & Zonen pyranometer, from 7:05 UT to 7:35 UT, is averaged for each day in Palaiseau and Carpentras; The data is kept when the standard deviation over 30 min is smaller than $30\,\mathrm{Wm}^{-2}$, indicating a cloudless sky.

4.1 $DSSF_{res}$

The case study period extends from 18 July 2003 to 19 August 2003 in Carpentras. 24 points remain available after the cloud-screening and are shown as empty circles in Fig. 4, representing $DSSF_{meas}$ in function of the day number in 2003. $DSSF_{meas}$ varies between 350 and $500\,\mathrm{Wm}^{-2}$. An approximate $80\,\mathrm{Wm}^{-2}$ decrease in 30 days is due to the decrease of the solar zenith angle at the constant time of 07:20 UT, from 65° to 60° (Fig. 2). This is shown by the red spotted line depicting the aerosol-free reference parameterised according to Eq. (1). As clouds are screened out from the data set, the features superimposed to the angular decline are induced by aerosols. Closest point to the spotted line occurs on 18 July indicating the minimum aerosol radiative effect during the time period. The difference between both curves increases

Aerosol radiative forcing over land from meteosat-7

T. Elias and J.-L. Roujean

Title Page

Abstract | Introduction

Conclusions | References

Tables | Figures

⏮ | ⏭

◀ | ▶

Back | Close

Full Screen / Esc

Printer-friendly Version

Interactive Discussion

EGU

from 19 to 23 July, reaches a secondary minimum between 28 July and 1 August, and increases again to 6 August. The difference stays large until 14 August.

$DSSF_{res}$ estimations are added in Fig. 4 as full circles. Main features are represented, as the first and second increase of the aerosol effect, and the minimal differences on 18 July, 31 July and 1 August. The histogram of the difference $DSSF_{res}$-$DSSF_{meas}$ is plotted in Fig. 5a. $DSSF_{meas}$ is reproduced within $10\,Wm^{-2}$ in 11 cases, within $20\,Wm^{-2}$ (around 5%) in 18 cases, which is 75% of the situations. The disagreement is not larger than $40\,Wm^{-2}$, which is around 10% of $DSSF_{meas}$. $DSSF_{par}$ (Eq. 1) is added in Fig. 4a for constant aerosol contribution $\delta=0.09$, and for $W=2.5\,gcm^{-2}$ and Uo3=300 DU. $DSSF_{par}$ generally underestimates $DSSF_{meas}$. The difference between $DSSF_{par}$ and $DSSF_{meas}$ (Fig. 5a) is included between $-10\,Wm^{-2}$ and $-40\,Wm^{-2}$ in 12 cases, and the difference is smaller than $-50\,Wm^{-2}$ in 7 cases (out of the axis). Figure 4 shows that the new method is an improvement to reproduce the high temporal variability of DSSF due to changing aerosol extinction properties.

The case study period extends from 7 July 2003 to 31 August 2003 in Palaiseau, when SZA varies from 59 to 69° at 07:20 UT. Cloud presence is more frequent as only 18 measurements are declared not affected by clouds. The histogram of the difference $DSSF_{res}$-$DSSF_{meas}$ plotted in Fig. 5b includes Carpentras and Palaiseau. The agreement remains within $20\,Wm^{-2}$ of $DSSF_{meas}$ in 70% of the situations. In three cases not plotted in Fig. 5b, the difference is included between -60 and $-50\,Wm^{-2}$, which is around 20% of the measurement. Nevertheless, the estimation is improved compared to the parameterisation for constant aerosol properties.

4.2 ARF_{res}

The ARF_{res} and ARF_{meas} estimates are calculated as the differences between $DSSF_{res}$ and $DSSF_{meas}$, respectively, and a reference level. The reference level in Carpentras and Palaiseau is defined for zero aerosol extinction ($\delta=0$), and for gas concentrations $W=2.5\,gcm^{-2}$ and Uo3= 300 DU, which gives a value larger by $11\,Wm^{-2}$ than

$DSSF_{meas}$ measured on 18 July 2003 in Carpentras, and larger by $17\,Wm^{-2}$ than $DSSF_{meas}$ measured on 22 August 2003 in Palaiseau. Estimates for Carpentras are plotted in Fig. 6 in function of the number of the day. We recognise the events already identified. ARF_{meas} is larger than $80\,Wm^{-2}$ on 6, 9 and 14 August and reaches
5   the maximum value of $100\,Wm^{-2}$ on 9 August. The agreement between ARF_{res} and ARF_{meas} is good, showing that the method is able to reproduce the main events.

Instantaneous aerosol optical thickness measured at 440 nm (AOT440), at the AERONET station of Carpentras at around 07:20 UT, is plotted in Fig. 7. AOT440 is smaller than 0.10 on 18 July, 30 July and 1 August, which correspond to minima
10   of ARF_{meas}, and AOT440 maxima are reached on 6 and 9 August, corresponding to ARF_{meas} maxima. This is a striking evidence that our satellite-based method is able to provide the aerosol radiative impact over land. The increase of AOT observed in Carpentras coincides with the 2003 summer heat wave and was also observed in Portugal (Elias et al., 2006), in the West Mediterranean Sea (Pace et al., 2005a; 2005b) and to
15   North-Western Europe (Hodzic et al., 2006).

4.3   ARFE

ARF_{res} and ARF_{meas} are plotted in function of AOT440 in Fig. 8a for Carpentras and in Fig. 8b for Palaiseau, and linear regressions are added. The slope of the linear regression is called the radiative forcing efficiency of the aerosols (ARFE). The agree-
20   ment in ARFE estimate is excellent between both methods. In Carpentras, ARFE is $143\,Wm^{-2}$/AOT440 for the ground-based measurements, and $124\,Wm^{-2}$/AOT440 for the satellite-based method. In Palaiseau, ARFE is $134\,Wm^{-2}$/AOT440 for the ground-based measurements, and $163\,Wm^{-2}$/AOT440 for the satellite-based method. The increase of AOT in Palaiseau is not only due to transport of biomass burning emissions
25   from Portugal (Hodzic et al., 2006), but also to urban influence from nearby Paris. This representation demonstrates that the algorithm is able to reproduce quantitatively the loss of solar energy due to the aerosols, at the surface level, at an instantaneous time

EGU

scale, over land, and without a further data set than the METEOSAT-7 visible channel. The algorithm is validated as ARF_{res} and AOT are two quantities obtained in a totally independent way, but still demonstrate a correlation consistent with theory. Estimations of ARFE in Carpentras and Palaiseau coincide to an accumulation-mode dominated and absorbent aerosol population (Fig. 3). This is consistent with the characteristics of the haze covering West Mediterranean, Portugal and France during the heat wave of the 2003 summer, and with urban pollution.

4.4 Temporal gradient of ARF

It is now studied the ability of the method in reproducing the temporal variability of ARF. Temporal gradient is calculated as the difference of ARF between 2 consecutive days. Satellite-based estimate is plotted in function of ground-based measurement in Fig. 9. Measured gradient varies between –40 and 30 Wm^{-2}. The signs of both temporal gradients are generally equal. The major benefit of the method is to detect from space the temporal tendency in aerosol radiative impact at the surface level over land. The linear regression is also plotted in Fig. 9, which shows that in average the temporal tendency is quantitatively reproduced with the satellite-based method.

5 Conclusions

A method is presented to estimate the solar radiative flux reaching the surface level (DSSF) and its temporal variability, as well as the aerosol radiative forcing at surface level (ARF), using the METEOSAT-7 visible broadband spectrum channel. The method consists in: 1) generating a Look Up Table of TOA radiance and DSSF with the 6S radiative transfer code; 2) discriminating between aerosol and surface contributions considering the dependence of the measurement on the solar zenith angle; 3) selecting the Surface Atmosphere Systems models able to reproduce the TOA radiance measurement, according to the inferred aerosol contribution; 4) averaging the DSSF values

computed from the candidate SAS models. The validation of the method relies on the comparison between satellite-based estimates and ground-based measurements for two case studies. The measurement conditions were variable: the solar zenith angle varies from 59 to 69°, the aerosol type varies from biomass burning to urban influence, the aerosol optical thickness varies by a factor of 6.

The satellite-based retrievals show a high correlation with the ground-based measurements of DSSF. The difference between the satellite-based estimates and the ground-based measurements is smaller than $20\,\mathrm{Wm^{-2}}$ and 5% of the signal, in 70% of the cases, and smaller than $40\,\mathrm{Wm^{-2}}$ in 90% of the cases. The method is also validated to infer the instantaneous radiative impact of aerosols over land, at ground level and in absence of cloud cover, as we show the excellent correlation between satellite-based estimate of the aerosol radiative forcing and ground-based measurement of aerosol optical thickness (AOT). They are two different quantities determined on a totally independent way, but still are related according to theory. Both satellite-based estimates and ground-based measurements show a strong sensitivity to AOT, with the Aerosol Radiative Forcing Efficiency (ARFE) included between 120 and $160\,\mathrm{Wm^{-2}}$ / AOT440. A wide scatter of ARFE is given in literature and more studies are necessary to define the bounds in function of the aerosol type. For example, ARFE is estimated for 2 days of SAFARI2000 by Hansell et al. (2003) at $200\,\mathrm{Wm^{-2}}$. Also, Zhou et al. (2005) compute ARFE for several aerosol types using the AERONET data base. Their estimate for biomass burning in South America is $70\,\mathrm{Wm^{-2}}$/AOT550 and $90\,\mathrm{Wm^{-2}}$/AOT550 for biomass burning emissions in South Africa. We also show that ARF can vary by as much as $\pm 40\,\mathrm{Wm^{-2}}$ in one day.

The next steps will consist: i) in defining the domain of validity of the method concerning the aerosol types (tests for desert dust) and the surface types (tests over highly reflecting surface as desert and snow); ii) in validating the estimation of the diurnal cycle of the radiative impact of different aerosol types. The major profit of the method will be to provide time series of realistic daily averages of the aerosol radiative impact in different environments (continental and maritime background, urban pollution, biomass

burning impacts), according to the cloud presence and the measured aerosol diurnal cycle. It is included in the objectives of the FP6/**geoland** project to draw continental maps of DSSF with the spatial resolution of 50 km and the temporal resolution of the hour, over the year 2000, using this method for clear-sky pixels and a parameterisation-based approach for the cloudy-sky pixels (Elias and Roujean, 2006).

This work takes part in the effort of the scientific community in lying the global estimates of aerosol radiative effects upon measurements, in order to improve the climate projections, and to close the aerosol issue on climate. Our method is complementary to other methods in the objective of providing a detailed picture of the aerosol radiative effect: our method may be combined with 1) TOMS identification of aerosol plumes characterised by high absorption properties; and with 2) identification of the aerosol type by the spatial missions as MODIS, MISR, POLDER, GLORY, SCIAMACHY, assuming the aerosol type does not change during the day.

Appendix A

$$K_{esd}=1.00011+0.034211 \cdot \cos(x) \tag{A1a}$$
$$+0.00128 \cdot \sin(x)+0.000719 \cdot \cos(2x)+7.7E-05 \cdot \sin(2x) \tag{A2a}$$

where $x=6.28 \cdot (nod-1)/365$ (A2b)

and nod is the number of the day in the year.

$$T=e^{-\frac{\delta}{\mu_S}}-A_{wv}(W/\mu_S)-A_{oz}(U_{o3}/\mu_S)-R_r(\mu_S) \tag{A3}$$

where U_{o3} is ozone concentration, W is water vapour concentration, δ is an aerosol extinction parameter, and μ_S is the cosine of the solar zenith angle.

$$A_{oz}(x) = \frac{0.02118x}{1+0.042x+0.000323x^2} + \frac{1.082x}{(1+138.6x)^{0.805}} + \frac{0.0658x}{(1+103.6x)^3} \tag{A4}$$

13519

$$A_{wv}(y) = \frac{2.9y}{(1 + 141.5y)^{0.635} + 5.925y} \qquad (A5)$$

$$R_r(\mu_S) = \frac{0.28}{1 + 6.43\mu_S} \qquad (A6)$$

Appendix List of acronyms

AE Angstrom Exponent
AERONET: AErosol RObotic NETwork
AOT: Aerosol Optical Thickness
AOT550: AOT at 550 nm
AOT_{min}: minimum value of AOT derived from TOA measurements
ARF: Aerosol Radiative Forcing
ARF_{res}: ARF estimated from METEOSAT-7 data set
ARFE: Aerosol Radiative Forcing Efficiency
a.s.l.: above sea level
ASD: Aerosol Size Distribution
ASSA: Aerosol Single Scattering Albedo
ATBD: Algorithm Theoretical Basis Document
BSRN: Baseline Surface Radiation Network
δ: aerosol extinction parameter
DSSF: Downwelling Surface Solar radiative Flux
$DSSF_{LUT}$: DSSF calculated by the 6S radiative transfer code for generating the LUT
$DSSF_{meas}$: ground-based measurement of DSSF
$DSSF_{par}$: parameterised DSSF
$DSSF_{res}$: DSSF estimated by the FP6/**geoland** method from the METEOSAT-7 data
E_{Sun}: extraterrestrial solar irradiance
FP6: 6th Framework Plan

GLORY

GMT: Greenwich Mean Time

GOCART: GOddard Chemistry Aerosol Radiation and Transport

IPCC: Intergovernmental Panel on Climate Change

5 IRI: Imaginary Refractive Index

K_{esd}: Earth-Sun distance correction factor

LUT: Look-Up Table

μ_S: cosine of SZA

MODIS: MODerate Imaging Spectrometer

10 MISR: Multiangle Imaging SpectroRadiometer

POLDER: POLarisation and Directionality of Earth Reflectance

SAFARI2000: South African Initiative

SAL: Surface ALbedo

SAL_{max}: FP6/**geoland** internal parameter describing the SAL maximum in the LUT

15 SAL_{mo}: FP6/**geoland** internal parameter describing the most occurring value of SAL in candidate SAS models

SAS: Surface Atmosphere System

SCIAMACHY: SCanning Imaging Absorption SpectroMeter for Atmospheric CHartographY

20 SZA: Solar Zenith Angle

T: atmospheric transmission

TOA: Top Of the Atmosphere

TOMS: Total Ozone Mapping Spectrometer

Uo3: ozone concentration

25 UTVR: Upwelling TOA Visible and near infra red Reflectance

$UTVR_{LUT}$: UTVR calculated by the 6S radiative transfer code for generating the LUT

$UTVR_{meas}$: UTVR measured by METEOSAT-7

W: water vapour concentration

References

Chung, E. C., Ramanathan, V., Kim D., and Podgorny, I. A.: Global anthropogenic aerosol direct forcing derived from satellite and ground-based observations, J. Geophys. Res., 110, D24, D24207, 2005.

Costa, M. J. and Silva, A. M.: Aerosol radiative forcing from GEO satellite data over land surfaces, in: Remote Sensing of Clouds and the Atmosphere X, edited by: K. P. Schäfer, A. Comerón, J. R. Slusser, R. H. Picard, M. R. Carleer, N. I. Sifakis, Proceedings of SPIE, Vol. 5979 (SPIE, Bellingham, WA), 582–589, 2005.

Elias, T. and Roujean, J. L.: ATBD Core Service biophysical Parameters - Downwelling surface Solar Radiation flux. Version 1.2, EC Proposal Reference FP–6–502871, 90 pp., 2006.

Elias, T., Silva, A. M., Belo, N., Pereira, S.,Formenti, P., Helas, G., and Wagner, F.: Aerosol extinction in a remote continental region of the Iberian peninsula during summer, J. Geophys. Res., 111, D14204, doi:10.1029/2005JD00, 2006.

Gautier, C., Diak, G., and Masse, S.: A simple physical model to estimate incident solar radiation at the surface from GOES satellite data, J. Clim. Appl. Meteorol., 19, 1005–1012, 1980.

Hansell, R., Tsay, S. C., Ji, Q., Liou, K. N., and Ou, S.: Surface aerosol radiative forcing derived from collocated ground-based radiometric observations during PRIDE, SAFARI, and ACE-Asia, Appl. Opt., 42, 27, 5533–5544, 2003.

Hodzic A., Vautard, R., Chepfer, H., Goloub, P., Menut, L., Chazette, P., Deuzé, J. L., Apituley, A., and Couvert, P.: Evolution of aerosol optical thickness over Europe during the August 2003 heat wave as seen from CHIMERE model simulations and POLDER data, Atmos. Chem. Phys., 6, 1853–1864, 2006, http://www.atmos-chem-phys.net/6/1853/2006/.

Holben, B. N., Tanré, D., Smirnov, A., et al., An emerging ground-based aerosol climatology: aerosol optical depth from AERONET, J. Geophys. Res., 106, 12 067–12 097, 2001.

Lacis, A. A. and Hansen, J. E.: A parameterization for the absorption of solar radiation in the Earth's atmosphere, J. Atmos. Sci., 31, 118–131, 1974.

Aerosol radiative
forcing over land
from meteosat-7

T. Elias and J.-L. Roujean

Title Page

Abstract	Introduction
Conclusions	References
Tables	Figures

◄ | ►

◄ | ►

Back | Close

Full Screen / Esc

Printer-friendly Version

Interactive Discussion

EGU

Pace, G., Meloni, D., and Di Sarra, A.: Forest fire aerosol over the Mediterranean basin during summer 2003, J. Geophys. Res., 110, D21202, 2005.

Schmetz, J.: Towards a surface radiation climatology: retrieval of downward irradiances from satellites, Atmos. Res., 23, 287–321, 1989.

Thieuleux, F., Moulin, C., Bréon, F. M., Maignan, F., Poitou, J., and Tanré, D.: Remote sensing of aerosols over the oceans using MSG/SEVIRI Imagery, Ann. Geophys., 23, 1–8, 2005, http://www.ann-geophys.net/23/1/2005/.

Vermote, E. F., Tanré, D., Deuzé, J. L., Herman, M., and Morcrette, J. J.: Second simulation of the satellite signal in the solar spectrum: An overview, IEEE Trans. Geosci. Remote Sens., 35, 675–686, 1997.

Yu, H., Kaufman, Y. J., Chin, M., Feingold, G., Remer, L. A., Anderson, T. L., Balkanski, Y., Bellouin, N., Boucher, O., Christopher, S., DeCota, P., Kahn, R., Koch, D., Loeb, N., Reddy, M. S., Schulz, M., Takemura, T., and Zhou, M.: A review of measurement-based assessments of the aerosol direct radiative effect and forcing, Atmos. Chem. Phys., 6, 613–666, 2006, http://www.atmos-chem-phys.net/6/613/2006/.

Zhou, M., Yu, H., Dickinson, R. E., Dubovik, O., and Holben, B. N.: A normalized description of the direct effect of key aerosol types on solar radiation as estimated from Aerosol Robotic Network aerosols and Moderate Resolution Imaging Spectroradiometer albedos, J. Geophys. Res. 110, D19, D19202, 2005.

Title Page

Abstract | Introduction

Conclusions | References

Tables | Figures

◄ | ►

◄ | ►

Back | Close

Full Screen / Esc

Printer-friendly Version

Interactive Discussion

EGU

Table 1. Range of values and increments of the geophysical input parameters of the 6S radiative transfer code, describing the SAS models, and varying for generating the LUT.

quantity	Acronym	range	increment	Number of values
Surface albedo	SAL	0.05–0.40	0.05	8
Aerosol optical thickness	AOT	0.05–1.50	0.1 from 0.10 to 1.50	16
Aerosol size distribution	ASD	3.50, 4.75	/	2
Aerosol absorption	IRI	0.001–0.030	0.014 and 0.015	3

EGU

Table 2. Successive operations to select candidate Surface-Atmosphere System models to determine $DSSF_{res}$.

Time of $UTVR_{meas}$	Condition on $UTVR_{LUT}$ $UTVR_{meas}$ cond	Condition on AOT_{LUT}	Condition on SAL_{LUT}	Operation on candidate values $DSSF_{LUT}$	Result	Time period validity of the retrieved parameter
noon	$0.9 \times UTVR_{meas} \leq$ $UTVR_{LUT} \leq 1.1 \times$ $UTVR_{meas}$	<1.0	none	averaging	$DSSF_{res}$ and SAL_{mo}	Instantaneous $DSSF_{res}$ & monthly value of SAL_{mo}
am	$0.9 \times UTVR_{meas} \leq$ $UTVR_{LUT} \leq 1.1 \times$ $UTVR_{meas}$	none	$SAL_{LUT} \leq$ SAL_{max} with $SAL_{max} = SAL_{mo}$ -0.10	/	AOT_{min}	Instantaneous AOT_{min}
am	$0.9 \times UTVR_{meas} \leq$ $UTVR_{LUT} \leq 1.1 \times$ $UTVR_{meas}$	$AOT_{min} - 0.1$ $\leq AOT_{LUT} \leq$ $AOT_{min} + 0.2$	none	averaging	$DSSF_{res}$	Instantaneous $DSSF_{res}$

EGU
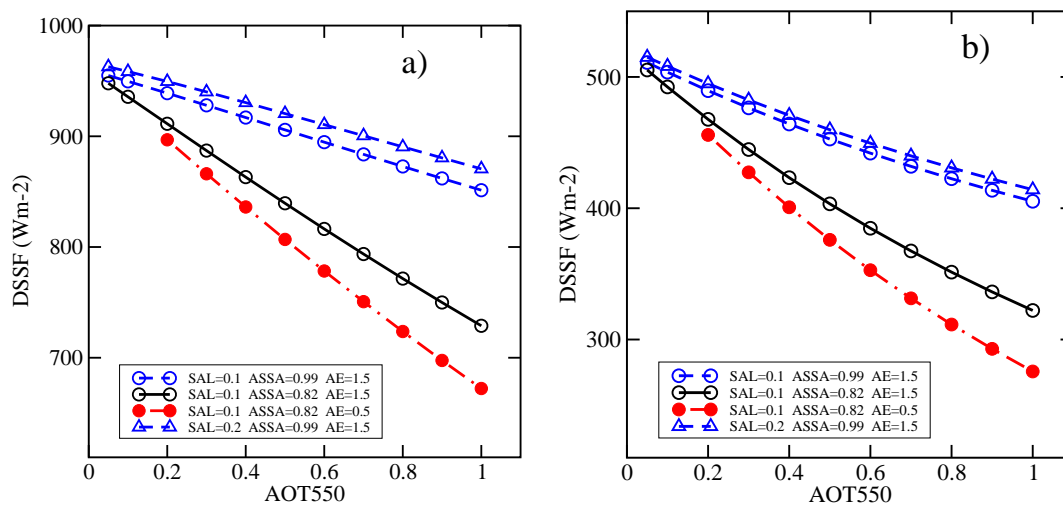
Fig. 1. Sensitivity of DSSF to AOT for two values of ASSA, two values of AE and two values of SAL. Simulations are made with the 6S code for **(a)** SZA=30° and **(b)** SZA=60°.
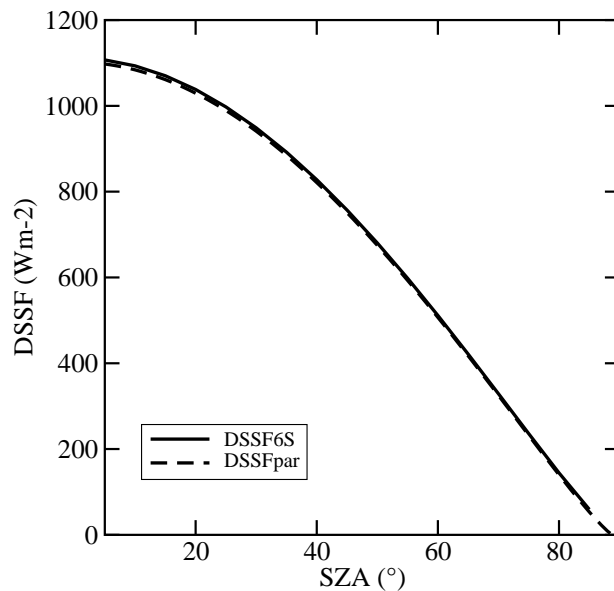
Fig. 2. Dependence of DSSF to SZA. 6S simulation and parameterisation for an aerosol-free atmosphere with 300 DU of ozone and $2\,g\,cm^{-2}$ of water vapour.

EGU
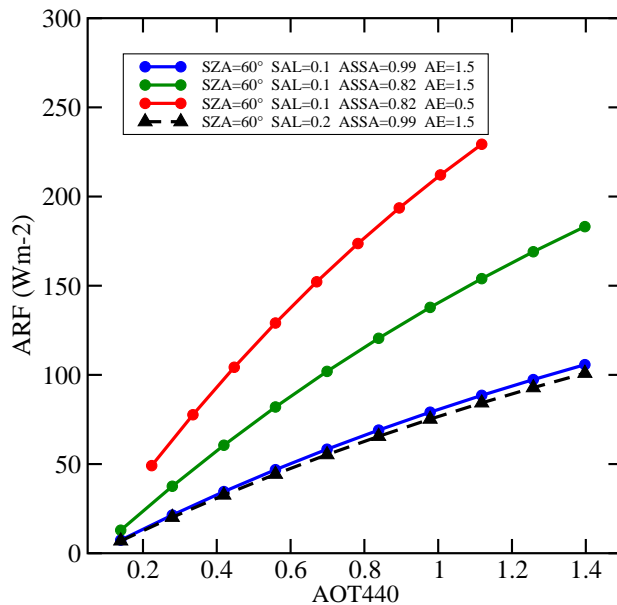
Fig. 3. Sensitivity of ARF to AOT440. ARF is computed with the 6S radiative transfer code for several aerosol models, and two values of SAL.
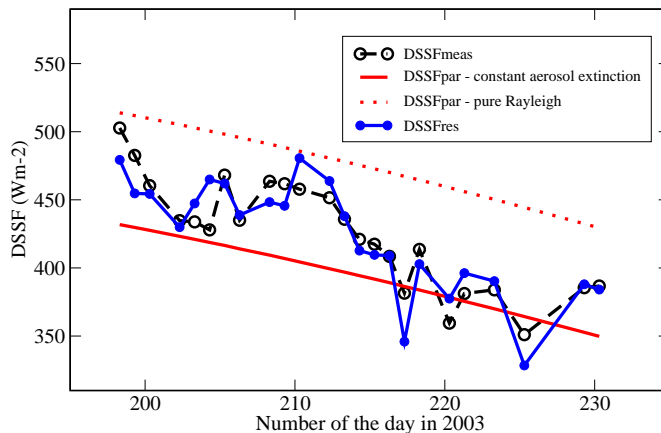
Fig. 4. Time series of DSSF$_{res}$, DSSF$_{meas}$, and DSSF$_{par}$ for Carpentras at 07:20 UT between 18 July 2003 and 19 August 2003. Parameterisation for pure Rayleigh is δ=0, W=2.5 g cm^{-2}, Uo3= 300 DU, parameterisation with aerosols is δ=0.09, W=2.5 g cm^{-2}, Uo3= 300 DU.

EGU
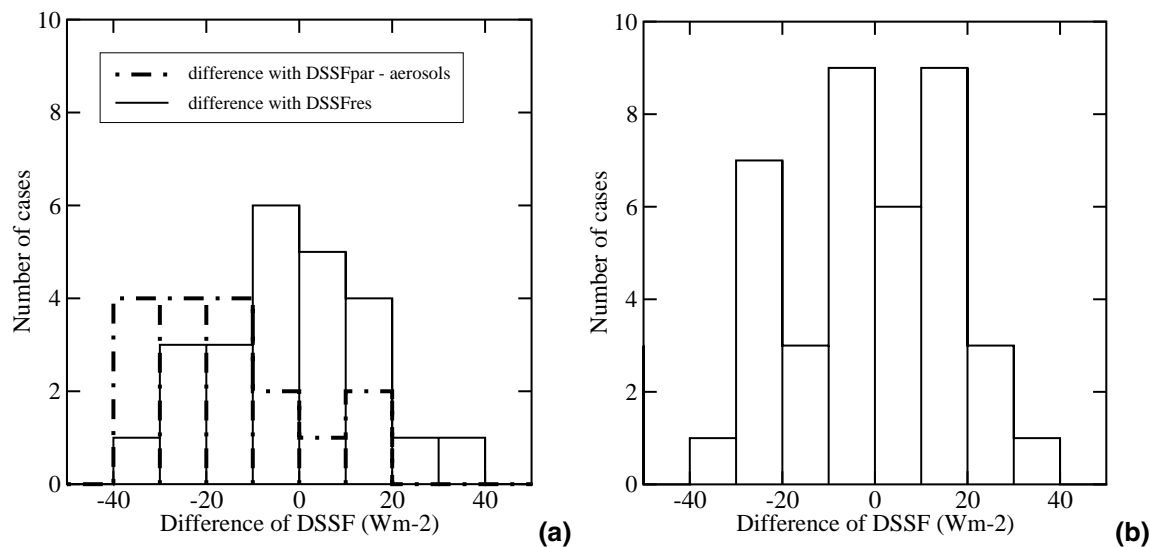
Fig. 5. (a) Histograms of the differences $DSSF_{par} - DSSF_{meas}$ and $DSSF_{res} - DSS_{meas}$, in Carpentras. **(b)** Histograms of the difference $DSSF_{res} - DSSF_{meas}$ for Palaiseau and Carpentras.
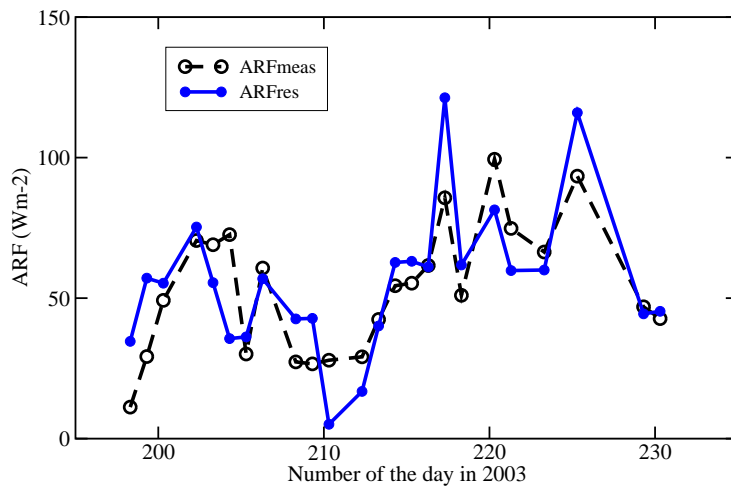
Fig. 6. Temporal series of the ground-based measurement and satellite-based estimate of ARF in Carpentras at 07:20 UT.

Title Page

Abstract | Introduction

Conclusions | References

Tables | Figures

◄◄ | ►►

◄ | ►

Back | Close

Full Screen / Esc

Printer-friendly Version

Interactive Discussion

EGU
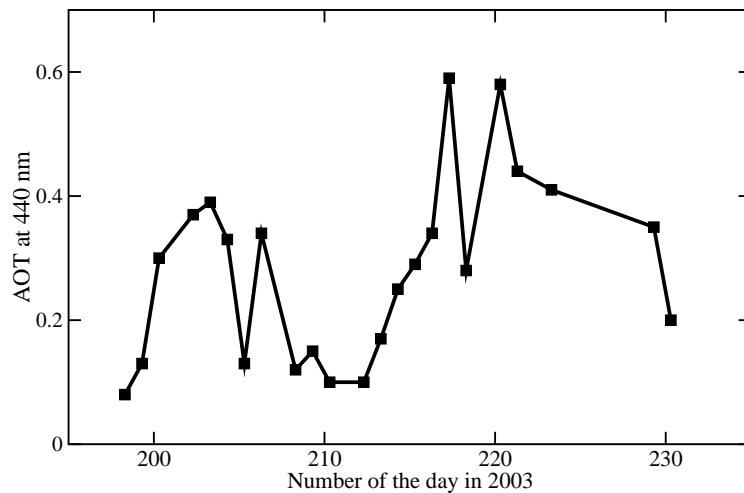
Fig. 7. Temporal series of the aerosol optical thickness measured at 440 nm at around 07:20 UT by AERONET at the station of Carpentras.
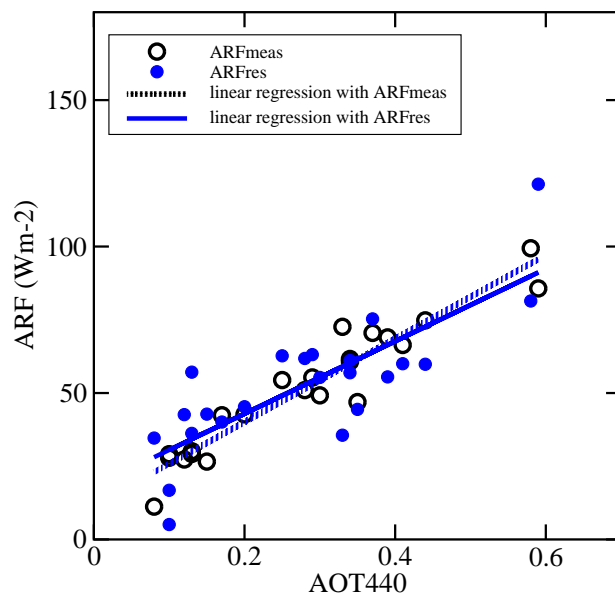
Fig. 8a. Sensitivity of the aerosol radiative forcing to the aerosol optical thickness in Carpentras. ARF is calculated from $DSSF_{meas}$ and from $DSSF_{res}$. Linear regressions are also plotted. The calculated slopes are (143 ± 10) Wm^{-2} with ARF_{meas} and (124 ± 21) Wm^{-2} with ARF_{res}.

EGU

EGU
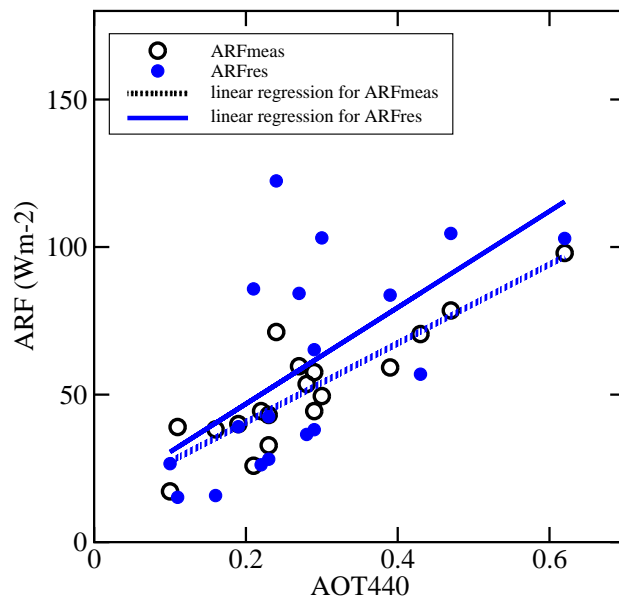
Fig. 8b. Idem as Fig. 8a but for Palaiseau. The calculated slopes are (134 ± 19) Wm^{-2} with ARF$_{meas}$ and (163 ± 53) Wm^{-2} with ARF$_{res}$.

EGU
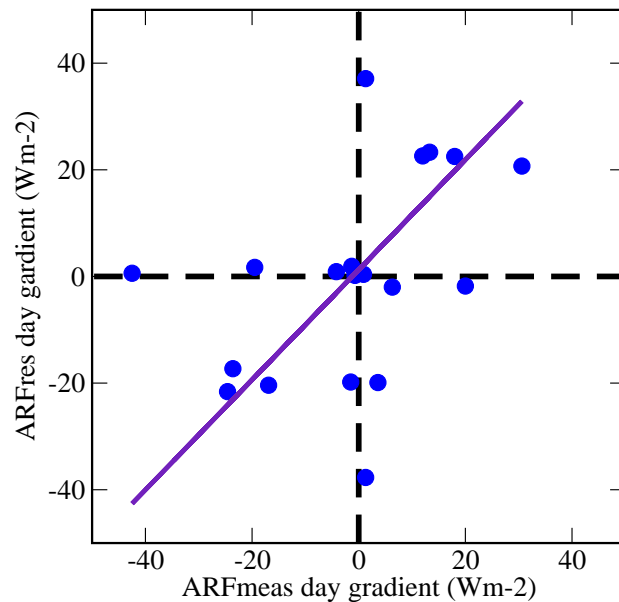
Fig. 9. Temporal gradient of ARF over one day in Palaiseau and Carpentras. Satellite based method against ground-based measurement estimate. Linear regression is also plotted.